

Directional-dependent coercivities and magnetization reversal mechanisms in fourfold ferromagnetic systems of varying sizes

T. Blachowicz, A. Ehrmann, P. Stebliński, and J. Palka

Citation: *J. Appl. Phys.* **113**, 013901 (2013); doi: 10.1063/1.4772459

View online: <http://dx.doi.org/10.1063/1.4772459>

View Table of Contents: <http://jap.aip.org/resource/1/JAPIAU/v113/i1>

Published by the [American Institute of Physics](#).

Related Articles

Magnetoresistance and shot noise in graphene-based nanostructure with effective exchange field
J. Appl. Phys. **112**, 123719 (2012)

Thermally assisted spin-transfer torque magnetization reversal in uniaxial nanomagnets
Appl. Phys. Lett. **101**, 262401 (2012)

Combined fitting of alternative and direct susceptibility curves of assembled nanostructures
J. Appl. Phys. **112**, 123902 (2012)

Thermal fluctuations of magnetic nanoparticles: Fifty years after Brown
App. Phys. Rev. **2012**, 13 (2012)

Thermal fluctuations of magnetic nanoparticles: Fifty years after Brown
J. Appl. Phys. **112**, 121301 (2012)

Additional information on J. Appl. Phys.

Journal Homepage: <http://jap.aip.org/>

Journal Information: http://jap.aip.org/about/about_the_journal

Top downloads: http://jap.aip.org/features/most_downloaded

Information for Authors: <http://jap.aip.org/authors>

ADVERTISEMENT



AIP Advances

Now Indexed in Thomson Reuters Databases

Explore AIP's open access journal:

- Rapid publication
- Article-level metrics
- Post-publication rating and commenting

Directional-dependent coercivities and magnetization reversal mechanisms in fourfold ferromagnetic systems of varying sizes

T. Blachowicz,^{1,a)} A. Ehrmann,² P. Stebliński,³ and J. Palka³

¹*Institute of Physics, Silesian University of Technology, 44-100 Gliwice, Poland*

²*Faculty of Textile and Clothing Technology, Niederrhein University of Applied Sciences, 41065 Mönchengladbach, Germany*

³*Faculty of Automatic Control, Electronics and Computer Science, Silesian University of Technology, 44-100 Gliwice, Poland*

(Received 23 June 2012; accepted 29 November 2012; published online 2 January 2013)

Different types of reversal processes, including either uniform-rotation or domain-wall driven processes, were identified in magnetic nano-wires of four-fold symmetry using micromagnetic simulations. Iron wires were tested for diameters ranging from 6 nm up to 20 nm, while their lengths were taken from 30 nm to 70 nm range, and for several directions of externally applied magnetic field. Physical parameters of presented low-dimensional structures enabled reversal via intermediate states, which can lead to additional stable states at remanence, contrary to unstable vortexes observed in magnetic nano-rings or cylindrical nanodots. © 2013 American Institute of Physics. [<http://dx.doi.org/10.1063/1.4772459>]

I. INTRODUCTION

The recent development of magneto-electronic devices is based on two main types of structural solutions. First, in a quite established and dominating way, the technology of ultra-thin ferromagnetic single layers and multilayers is used in laboratories and commercial markets. Second, promising candidates for the next generation of information storage media and sensing devices are intensively studied in periodical arrays of single ferromagnetic circular or wired nano-objects. Such multilayered cylindrical systems are applied in magnetic random access memories (MRAM)¹ and generally in spin valves.^{2,3} The wire-based approach, however, being inspired by textile magnetic materials⁴ or low-dimensional magnetocrystalline symmetries observed in epitaxial layers,⁵ can offer novel magnetic shape anisotropies at micro-scale and also many scenarios for magnetization dynamics. Thus, this topic requires systematic research to warrant a deep understanding of the appearing phenomena.

In the recent literature, there are some interesting reports of exotic magnetic states in wire-arrays and single objects. For example, stable onion states were examined in permalloy (Py) rectangular rings of size $1.5 \mu\text{m} \times 1 \mu\text{m}$, with a rectangular cross-section of $250 \times 250 \text{ nm}^2$, by Subrami *et al.*⁶ Wang *et al.* tested rectangular arrays of $1.15 \mu\text{m} \times 0.7 \mu\text{m}$ rings with a closely (100 nm) and a widely (500 nm) spaced option for packing,⁷ and concluded that closer spacing influences transitions from vortex states into onion states and vice versa, due to more collective behavior of rings. Interesting systems of closely spaced squared Py dipole lattices of four-fold symmetry and iron (Fe) Kagome lattices (a special composition of interlaced triangles) of six-fold symmetry, interacting via dipolar fields, were studied by Remhof *et al.*⁸ and Westphalen *et al.*⁹ Importantly, they observed collective

effects and interpreted occurrence of horseshoe and vortex states in terms of interactions between parallel and anti-parallel magnetically ordered sublattices. Gao *et al.* also reported a rich set of magnetic states.¹⁰ They observed different routes for magnetization evolution including transitions between a domain wall, diagonal onion, horseshoe, and a transition leading to vortexes in deformed cobalt (Co) rings, which were 880 nm in length along the major axis and 660 nm along the minor axis, and with ring width of 300 nm and an inter-ring edge-to-edge spacing of 500 nm. In his interpretation, Gao emphasized that the difference between easy and hard directions for a reversal analysis originated mainly from the dynamics of a single object in a relatively far spaced array, when the influence of magnetic stray fields can be less significant. A similar search for novel magnetic states, narrowed to single magnetic objects, was carried out by He *et al.* in a slotted Co nanoring.¹¹ The slotting was applied to break closed flux of vortexes and the analysis was only carried out for the two main orientations of an externally applied magnetic field equivalently to a hard and an easy directions. Zang and Haas studied a magnetic nanocylinder using Monte Carlo analysis of switching behavior influenced by shape modifications.¹² Recently, Yoon *et al.* analyzed tail-to-tail domain wall motion in a circular ring made from a wire to reveal a spin-valve behavior.¹³ Finally, an analysis of a single quaternary wire system, used as a possible four-states memory cell, was carried out by the authors.¹⁴

One of the most important issues occurring in magnetic nanosamples is the problem of stability of magnetic states during evolutions between saturation and anti-saturation, including analysis of states at remanence. In this paper, we narrow our analysis to single magnetic squared objects made from Fe wires, being inspired by textile magnetic materials. Tests of different side lengths (30 nm–70 nm) and different length-to-diameter ratios (~ 3 –11), carried out for several angular in-plane directions of externally applied field,

^{a)}Author to whom correspondence should be addressed. Electronic mail: tomasz.blachowicz@polsl.pl.

ranging from 0° to 45° , resulted in occurrence of stable and unstable magnetic states and novel scenarios for magnetization dynamics.

We show that an intermediate state—recognized by a step in hysteresis process—can lead to the stable remanent state existing for zero-valued magnetic field, for which the remanent magnetization is less than the remanent magnetization of the main hysteresis loop.¹⁴ For quaternary systems, those states at remanence were also observed, and importantly, they were achievable reversely by sequentially switching off the magnetic field vector.

In the subsequent chapters, we provide color-coded histograms of coercivities, which reveal magnetic states showing spatial distributions of magnetization vectors at remanences and for field coercivity moments. Next, we present hysteresis curves obtained for six different magnetization reversal mechanisms, and finally analyze exchange energy as a function of externally applied magnetic field for all of these scenarios. Simulations were carried out in order to systemize the recent findings of intermediate stable states in quaternary wire system.¹⁴

II. MODELLING

Using a micromagnetic simulator¹⁵ based on a finite element mesh and Landau-Lifshitz-Gilbert (LLG)¹⁶ equation of magnetization dynamics evolution, we investigated square systems of four Fe wires crossed at the ends. Tetrahedral meshes, prepared by the GiD personal pre and post processor elaborated in the International Center for Numerical Methods in Engineering (Barcelona, Spain), had typical sizes of 3 nm, understood as a distance between nodal points, which is less than the Fe Néel exchange length of 3.69 nm,¹⁷ which warrants proper micromagnetic calculation results. The diameters of tested wires in a square configuration, superimposed at the ends, are chosen between 6 nm and 20 nm and the lengths between 30 nm and 70 nm. The length/diameter aspect ratio of the wires determined the volume of crossing regions and mainly influenced the resulting demagnetizing fields. The other material parameters were chosen as follows: exchange constant $A = 2 \times 10^{-11}$ J/m, magnetic polarization at saturation $J_s = 2.1$ T, the Gilbert damping constant $\alpha = 0.1$, and the energy-density anisotropy constants $K_1 = 4.8 \times 10^4$ J/m³, $K_2 = 5.0 \times 10^3$ J/m³.¹⁸ Similar lateral sizes (50–300 nm) were often used in recent theoretical articles about magnetic nano-particles.^{11,16,19–24} The slightly smaller dimensions considered here additionally exhibit interesting effects which have to be taken into account when our findings are to be transferred to applied solutions. To enhance the possibility of comparison of the square system under investigation with nano-patterned rings,^{11,12,25–27} we have chosen an in-plane oriented sample instead of perpendicularly oriented ferromagnetic regions as used in today's hard disks.

In general, assumed physical conditions and spatial parameters are equivalent to nanocrystalline samples, since micromagnetism deals with the sample shape and microstructure. It results from the fact that the micromagnetic method is based on the conception of a magnetic particle and works at scales between crystalline lattices and domain

walls. Thus, it is able to simulate granular and polycrystalline microstructures with random magnetocrystalline anisotropy, material inhomogeneities, and irregular magnetic regions.

In order to obtain a hysteresis and observe magnetization reversal mechanism, a magnetic wire-system has been simulated using the external magnetic field H_{ext} , lying in the sample plane, which was swept from 0 to 600 kA/m at a constant speed of 10 kA/(m ns), then swept back at the same speed to -600 kA/m, and oriented back to positive saturation again. The field sweeping speed was chosen along the lines of typical values for MRAM applications.²⁸ Tests with a slower sweep rate, 1 kA/(m ns), did not show significant changes in the results. Importantly, even for the higher sweep rate ripples, understood as high-frequency oscillations (GHz) of the magnetization vector with characteristic small amplitudes that do not strictly correlate with a smooth vector evolution, were not observable in the presented wire samples.

III. RESULTS

Fig. 1 depicts the results of the coercivities, for different lengths-to-diameter ratios, for different orientations of the externally applied magnetic field—the color code shows the coercive fields of the respective simulations in (kA/m) unit. Comparing the graphs for the different orientations, it is obvious that 0° and 45° cases (associated with symmetry axes) show similar results, while simulations for other angles are different. For 0° and 45° results (Fig. 1), the largest coercivities can be found for systems with short and thin wires, and the smallest coercivities occur for systems of wires with larger diameters, almost independent of the wire length (different colors are roughly oriented horizontally). Changing the field orientations, from 0° to 5° and from 45° to 40° values, modifies the coercivity characteristics significantly (Fig. 1) making comparable coercivity regions oriented more diagonally.

In order to test numerical stability and to avoid unintentional artifacts in hysteresis loops, we compared 0° and 45° results with those obtained for slightly tilted directions of the applied field, that is, for 1° and 44° orientations, respectively. The results indicate that 0° is an unstable direction in the simulation, changing the effects found here very fast for directly neighboring directions for all tested samples. On the other hand, the 44° result shows a qualitatively similar tendency only for samples of relatively small dimensions. In that sense, the 45° direction is a stable direction in the simulation.

The strong quantitative differences of the coercivities for different wire lengths and diameters lead to the idea that different magnetization reversal processes may occur for different orientations and dimensions of the wire systems. Indeed, the magnetization snapshot of the simulations shows several different magnetization reversal mechanisms, which are indicated exemplarily in Fig. 1, i.e., undisturbed vortex states, vortex state deformed by an out-of-plane component, coherent magnetization reversal, horseshoe and deformed horseshoe states, deformed onion states, and domain wall

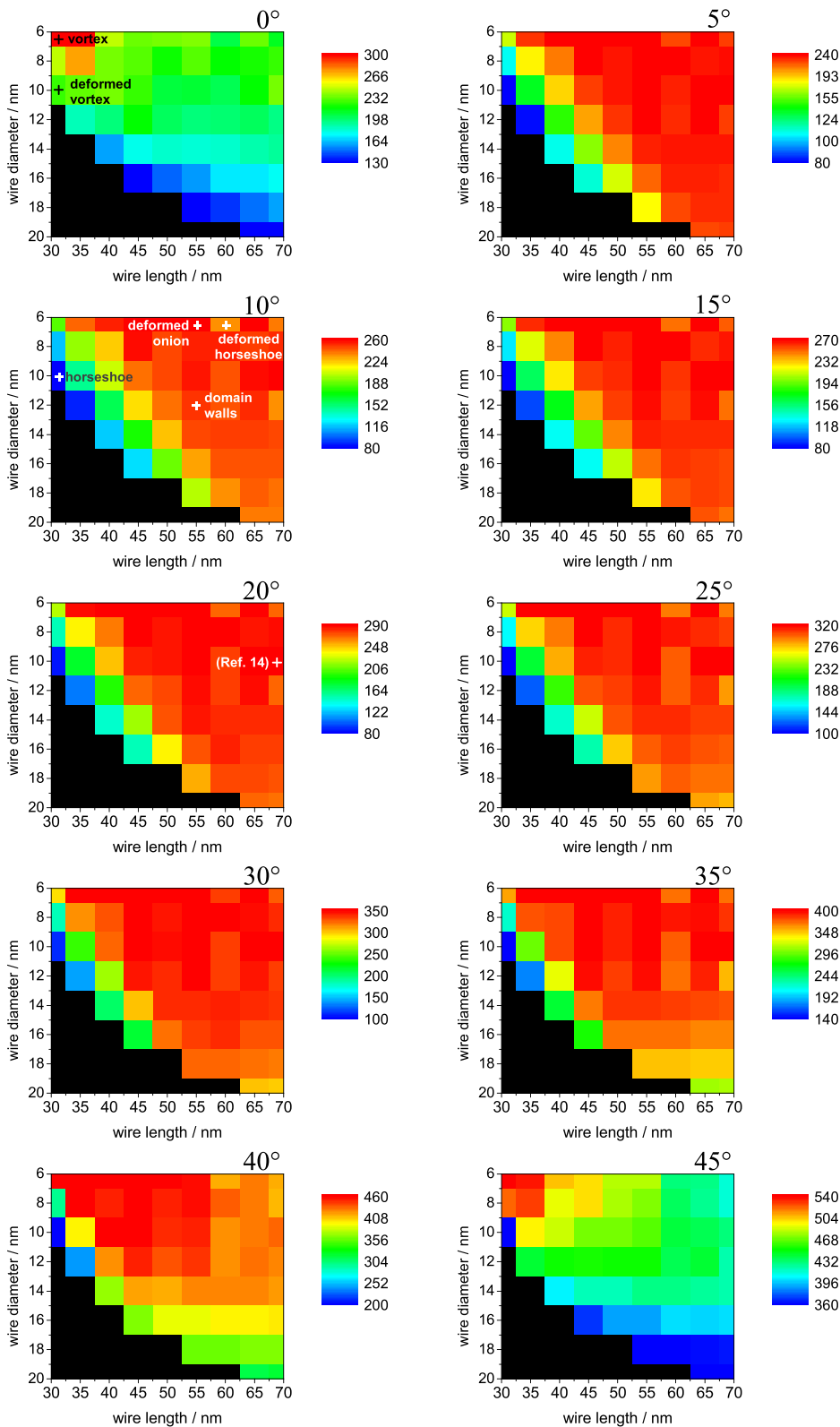


FIG. 1. Color-coded plot of coercivities, simulated for different orientations of externally applied magnetic field in (x - y) plane—the angle measured between the magnetic field intensity vector and the x -axis (compared to Fig. 2): 0° with the position of evolution with vortex, and of evolution with disturbed vortex, 10° with the positions of evolution with coherent magnetization reversal and dominating horseshoe states, via deformed horseshoe, via deformed onion state, and with domain-wall process and intermediate states excluded marked by crosses, respectively; 20° with the position of the Ref. 14 marked by a cross. The coercivity scale is expressed in (kA/m) units. Black regions point on non-simulated configurations.

nucleation and propagation processes. Additionally, the system used in a former examination¹⁴ is marked in Fig. 1 for 20° field orientation, where onion states were observable.

Examples of all magnetization states are given later in Fig. 2. The graphs depict snapshots of different magnetization reversal processes which have been found in the samples under simulation, together with the hysteresis loop of the

respective system and hysteretic changes of exchange energy density. Figs. 2(a) and 2(b) show different possibilities of magnetization reversal for a system orientation adjusted to 0° (i.e., with one pair of wires parallel to the external magnetic field), via a vortex state (state marked as II in Fig. 2(a)), leading to a step in the hysteresis loop (an intermediate state), or by a similar state with an out-of-plane

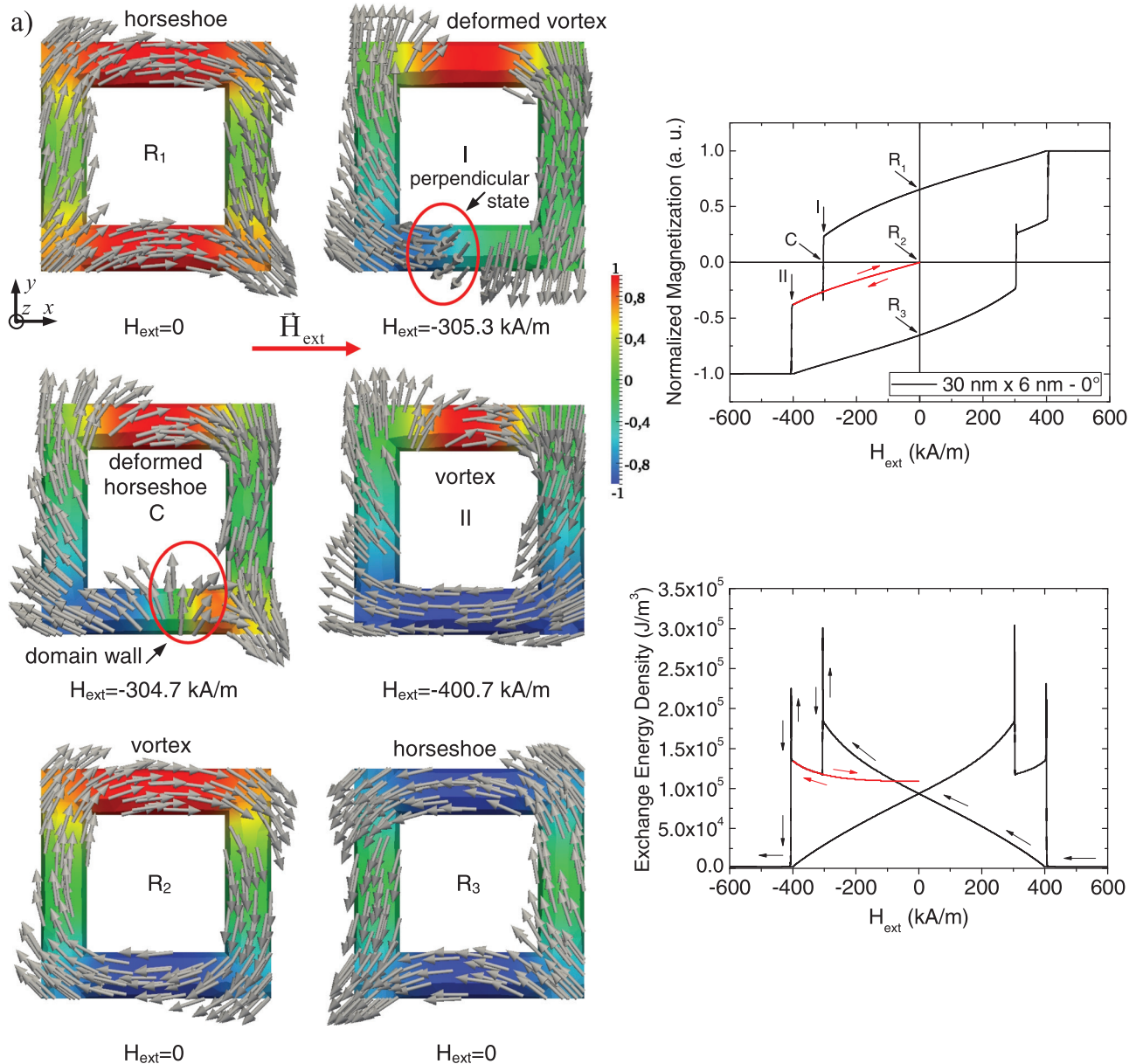


FIG. 2. Magnetization reversal mechanisms and the associated characteristic magnetization states: vortex in $30 \text{ nm} \times 6 \text{ nm}$ (length \times diameter) system with 0° orientation (a), out-of-plane magnetization component (domain wall) and disturbed vortex in $30 \text{ nm} \times 10 \text{ nm}$ system with 10° orientation (b), coherent magnetization reversal in $30 \text{ nm} \times 10 \text{ nm}$ system with 10° orientation and existence of horseshoe states (c), deformed horseshoe state in $60 \text{ nm} \times 6 \text{ nm}$ system with 10° orientation (d), deformed onion state in $55 \text{ nm} \times 6 \text{ nm}$ system with 10° orientation (e), and domain wall nucleation and propagation in $55 \text{ nm} \times 12 \text{ nm}$ system with 10° orientation (f). Hysteresis loops are given with the marked positions of magnetization states. The samples were colored in accordance with M_x magnetization vector component orientation, when the component is parallel (red), anti-parallel (blue), or perpendicular (green) to the direction of externally applied magnetic field. The exchange energy density as a function of externally applied field shows transient effects for all cases ((a)–(f)), for coherent reversal is very nonlinear (c). For reversals with disturbed horseshoes and onions ((d) and (e)), main remanent states and intermediate stable states have the same exchange energy. For evolution with vortices (a) and for coherent reversal (c), the exchange energy for stable intermediate states predominates over the energy of the main remanent states. Inequality of spike amplitudes for some cases results from resolution of numerical procedures.

magnetization component (marked as C in Fig. 2(b)), leading to a hysteresis loop without steps, respectively.

The additional four processes have also been found in simulated systems rotated away from 0° : the coherent magnetization reversal via horseshoe states and leading to the same horseshoe at stable intermediate state (marked as R_2 in Fig. 2(c)), only occurring in small particles with relatively thick wires; the reversal via deformed horseshoe states and domain walls at coercivity field (C) leading to a stable intermediate state (R_2) as a horseshoe one (Fig. 2(d)); next, the similar reversal via deformed onion states and domain walls

at coercivity field (C) leading to a stable intermediate state (R_2) as an onion one (Fig. 2(e)), which are often seen in larger systems with relatively thinner wires; and finally, the reversal via domain walls nucleated and propagated along wires observable in particles of all dimensions (Fig. 2(f)). The reversal processes leading to stable intermediate states—i.e., coherent rotation, horseshoe, and onion state—can be recognized by steps in the hysteresis loops (in some cases not very broad or with a magnetization component M_x quite near to the saturation magnetization) as it can be seen in Figs. 2(c)–2(e). No step occurs in reversal with vortex

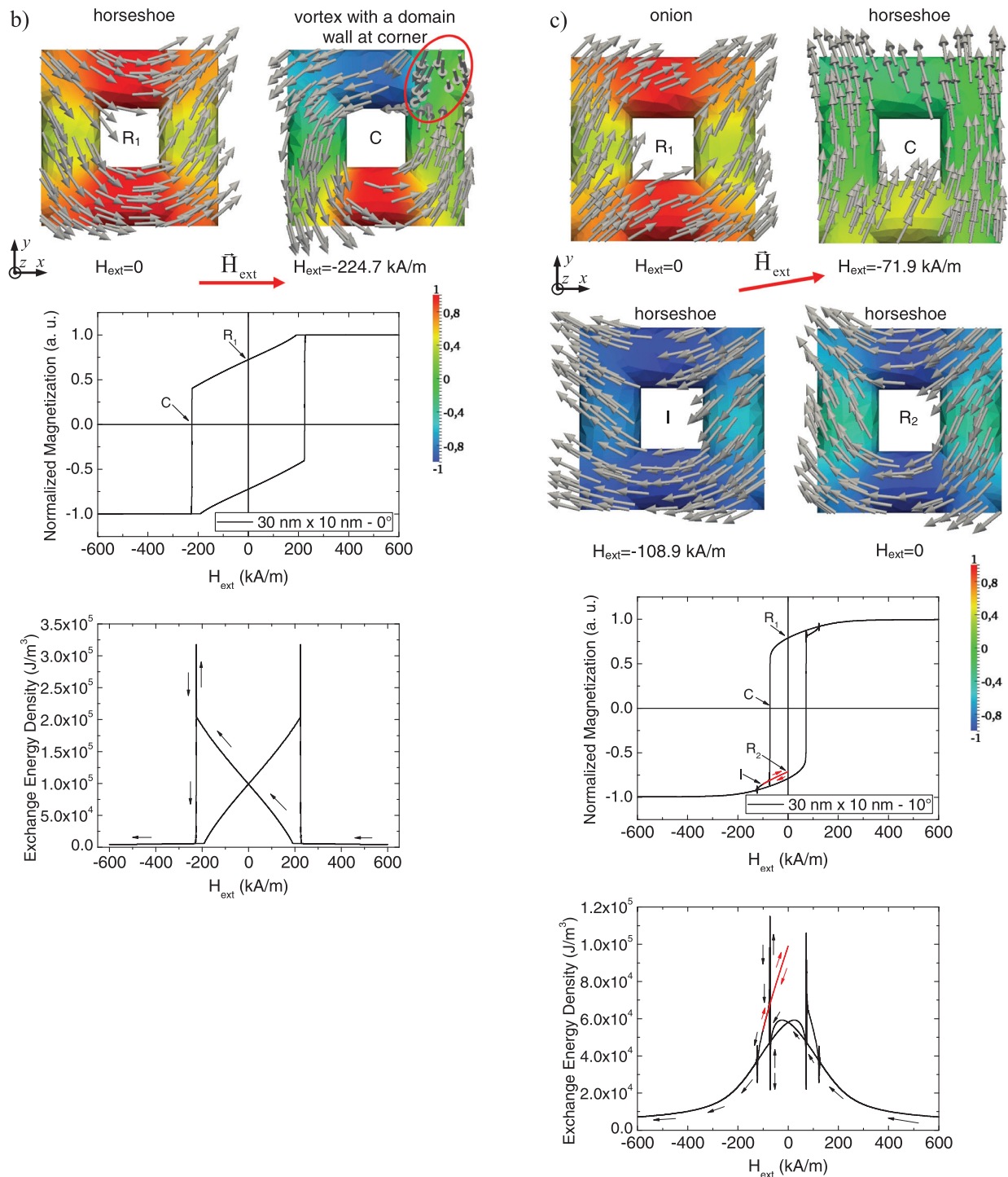


FIG. 2. (Continued.)

disturbed by a domain wall (Fig. 2(b)) and domain wall dominated processes (Fig. 2(f)).

It should be mentioned that in some samples, the magnetization reversal process is performed by more than one of the above described processes, sometimes leading to two separate steps on either side of a hysteresis loop or other effects which are not described here in detail.

Another characteristic useful for reversal process distinction is based on the analysis of exchange the energy density, driven by the externally applied magnetic field. There are three main features discovered in the analyzed samples.

First, the exchange energy for a stable intermediate state (if it exists) can be larger than that of remanences state, for evolution with dominating vortices (Fig. 2(a)) or for uniform rotation with dominating horseshoes (Fig. 2(c)). Second, the exchange energy at stable intermediate states can be equal to the exchange energy for a state at the main hysteresis loop remanence, when evolution is guided by horseshoes or onions disturbed by occurrence of domain walls, seen at the coercivity (Figs. 2(d) and 2(e)). Third, for rapid magnetization reversal moments, when magnetization changes its sign near the coercivity, exchange energy evolves via sharp

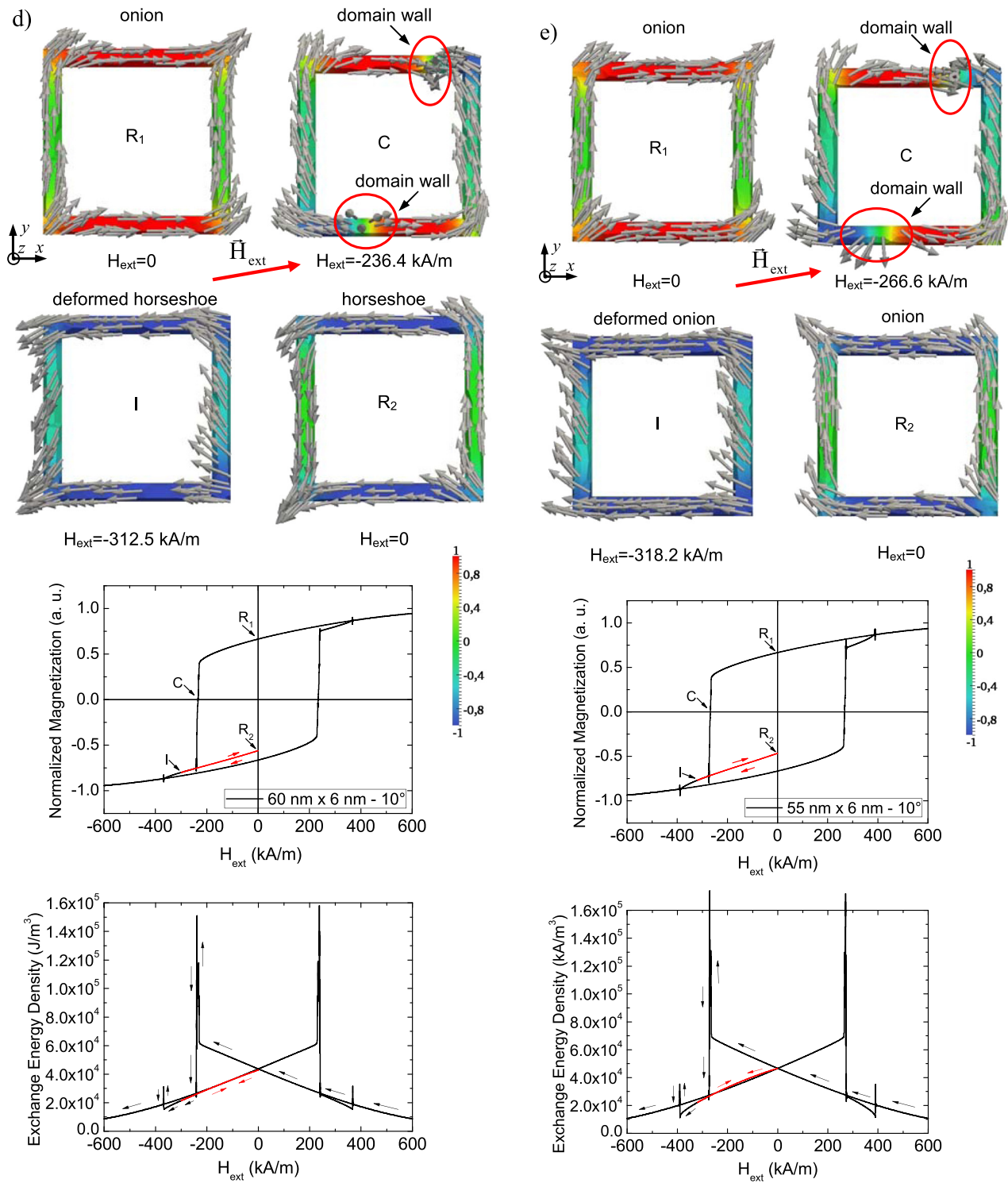


FIG. 2. (Continued.)

transient states. This effect is common for all considered samples and configurations. Additionally, extra exchange energy spikes can be found for the cases with steps, when magnetization features local rapid change evolving from an intermediate step into a main hysteresis loop. It is also worth to mention that for some situations, the system evolution, expressed by the exchange energy, can be sometimes highly nonlinear, which is a characteristic feature of uniform reversal processes (Fig. 2(c)).

IV. CONCLUSIONS

To conclude, we have shown by micromagnetic simulations that the fourfold wire systems under examination exhibit six different types of reversal processes, depending on system dimensions and orientation to the external magnetic field. For reversal processes along intermediate states, the corresponding hysteresis loops exhibit a step. A broad overview over the possible combinations of wire dimensions

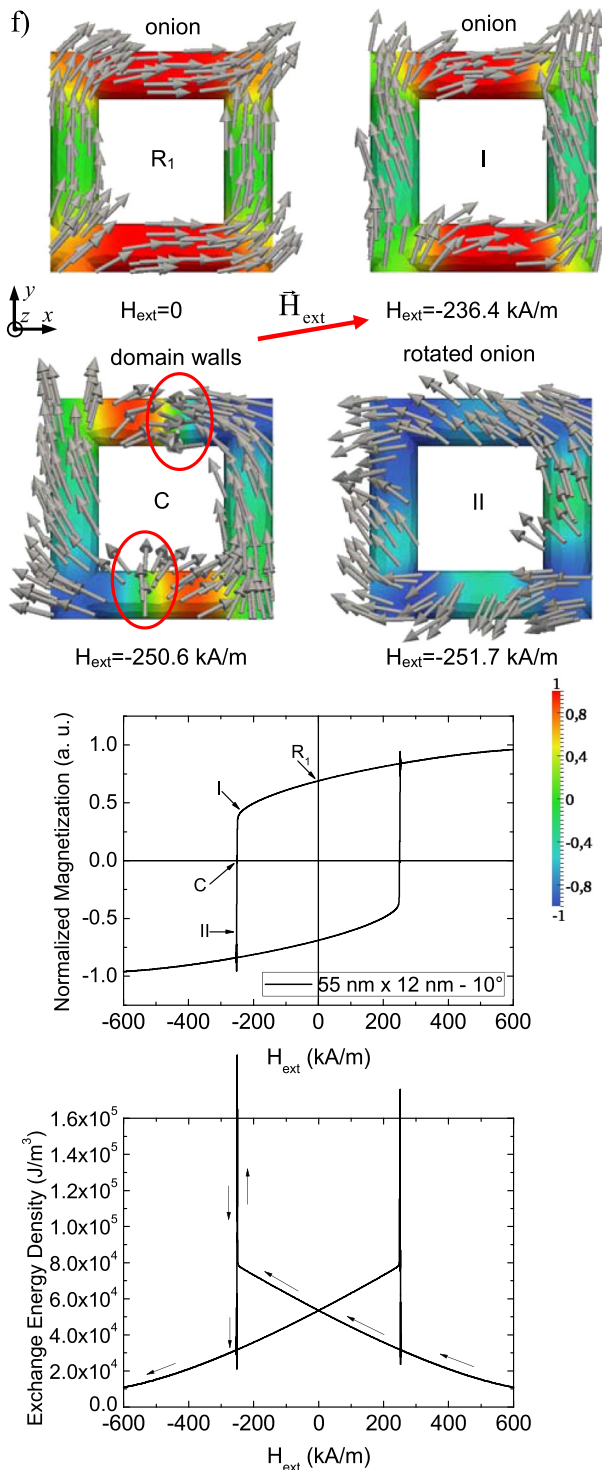


FIG. 2. (Continued.)

and orientations results in the finding that for highly symmetric orientations, i.e., 0° and 45° , the dimensional dependence of the coercive fields—diameter vs. length diagrams—is nearly opposite to that in less symmetric orientations. In other words, the less symmetric orientations are more susceptible to magnetization reversal via intermediate states. The susceptibility for such reversal in magnetic wire nanostructures is possible for a rich set of samples dimensions visible as separate regions derived from coercivity character-

istics. Taking advantage from the competition between exchange and demagnetizing fields at nanoscale, it was shown that this effect can be tailored by a shape modification (length-to-diameter-ratio) indicating possible applications in next generation memory devices based on patterned structures.

ACKNOWLEDGMENTS

The project has partly been funded by the Internal Project Funding of Niederrhein University of Applied Sciences.

- ¹Ch. Vogler, F. Bruckner, M. Fuger, B. Bergmaier, T. Huber, J. Fidler, and D. Suess, *J. Appl. Phys.* **109**, 123901 (2011).
- ²U. Roy, H. Seinige, F. Ferdousi, J. Mantey, M. Tsoi, and S. K. Banerjee, *J. Appl. Phys.* **111**, 07C913 (2012).
- ³S. Yoon, Y. Jang, Ch. Nam, S. Lee, J. Kwon, K. Na, K. Lee, and B. K. Cho, *J. Appl. Phys.* **111**, 07E504 (2012).
- ⁴A. Tillmanns, M. O. Weber, T. Blachowicz, L. Pawela, and T. Kammermeier, in Proceedings of the IV European Conference on Computational Mechanics, ECCM 2010, Palais des Congrès, Paris, France, 16-21 May 2010.
- ⁵T. Blachowicz, A. Tillmanns, M. Fraune, R. Ghadimi, B. Beschoten, and G. Güntherodt, *Phys. Rev. B* **75**, 054425 (2007).
- ⁶A. Subramani, D. Geerapuram, A. Domanowski, V. Baskaran, and V. Metlushko, *Physica C* **404**, 241 (2004).
- ⁷J. Wang, A. O. Adeyeye, and N. Singh, *Appl. Phys. Lett.* **87**, 262508 (2005).
- ⁸A. Remhof, A. Schumann, A. Westphalen, H. Zabel, N. Mikuszeit, E. Y. Vedmedenko, T. Last, and U. Kunze, *Phys. Rev. B* **77**, 134409 (2008).
- ⁹A. Westphalen, A. Schumann, A. Remhof, H. Zabel, M. Karolak, B. Baxevanis, E. Y. Vedmedenko, T. Last, U. Kunze, and T. Eimüller, *Phys. Rev. B* **77**, 174407 (2008).
- ¹⁰X. S. Gao, A. O. Adeyeye, S. Goolaup, N. Singh, W. Jung, F. J. Castañón, and C. A. Ross, *J. Appl. Phys.* **101**, 09F505 (2007).
- ¹¹K. He, D. J. Smith, and M. R. McCartney, *J. Appl. Phys.* **107**, 09D307 (2010).
- ¹²W. Zhang and S. Haas, *Phys. Rev. B* **81**, 064433 (2010).
- ¹³S. Yoon, Y. Jang, K.-J. Kim, K.-W. Moon, J. Kim, Ch. Nam, S.-B. Choe, and B. K. Cho, *J. Appl. Phys.* **111**, 07B910 (2012).
- ¹⁴T. Blachowicz and A. Ehrmann, *J. Appl. Phys.* **110**, 073911 (2011).
- ¹⁵W. Scholz, J. Fidler, T. Schrefl, D. Suess, R. Dittrich, H. Forster, and V. Tsiantos, *Comput. Mater. Sci.* **28**, 366 (2003).
- ¹⁶T. L. Gilbert, *IEEE Trans. Magn.* **40**, 3443 (2004).
- ¹⁷W. Scholtz, *Scalable Parallel Micromagnetic Solvers for Magnetic Nanostructures*, Ph.D. dissertation (2003), p. 161.
- ¹⁸E. F. Kneller and R. Hawig, *IEEE Trans. Magn.* **27**, 3588 (1991).
- ¹⁹J. Moritz, G. Vinai, S. Auffret, and B. Dieny, *J. Appl. Phys.* **109**, 083902 (2011).
- ²⁰A. L. Dantas, G. O. G. Rebouças, and A. S. Carrico, *IEEE Trans. Magn.* **46**, 2311 (2010).
- ²¹Y. Li, T. X. Wang, and Y. X. Li, *Phys. Status Solidi B* **247**, 1237 (2010).
- ²²B. Zhang, W. Wang, C. Mu, Q. Liu, and J. Wang, *J. Magn. Magn. Mater.* **322**, 2480 (2010).
- ²³J. Mejía-López, D. Altbir, P. Landeros, J. Escrig, A. H. Romero, I. V. Roshchin, C.-P. Li, M. R. Fitzsimmons, X. Battle, and I. K. Schuller, *Phys. Rev. B* **81**, 184417 (2010).
- ²⁴I. Tudosa, J. A. Katine, S. Mangin, and E. E. Fullerton, *Appl. Phys. Lett.* **96**, 212504 (2010).
- ²⁵R. P. Cowburn, D. K. Koltsov, A. O. Adeyeye, M. E. Welland, and D. M. Tricker, *Phys. Rev. Lett.* **83**, 1042 (1999).
- ²⁶J. G. Zhu, Y. F. Zheng, and G. A. Prinz, *J. Appl. Phys.* **87**, 6668 (2000).
- ²⁷F. Q. Zhu, D. L. Fan, X. C. Zhu, J. G. Zhu, R. C. Cammarata, and C. L. Chien, *Adv. Mater.* **16**, 2155 (2004).
- ²⁸S. Tehrani, B. Engel, J. M. Slaughter, E. Chen, M. DeHerrera, M. Durlam, P. Naji, R. Whig, J. Janesky, and J. Calder, *IEEE Trans. Magn.* **36**, 2752 (2000).